Nonplanar surface characterization by acoustic microscopy

M. Poirier, M. Castonguay, C. Neron,[a] and J. D. N. Cheeke,
Département de Physique, Université de Sherbrooke, Sherbrooke, J1K 2R1 Québec, Canada

(Received 17 June 1983; accepted for publication 13 September 1983)

We report the measurement of the acoustic material signature (AMS), amplitude and phase, on planar and nonplanar surfaces. The one-dimensional AMS is then used simultaneously with the scanning mode of the acoustic microscope to obtain the acoustic images of nonplanar surfaces. This technique is shown to be useful to test the quality of small spherical cavities used in the acoustic lenses fabrication, and also to characterize subsurface defects. This technique is based on the interpretation of fringe patterns appearing in the acoustic images.

PACS numbers: 43.35.Sx, 68.25. + j, 68.20. + t

I. INTRODUCTION

The scanning acoustic microscope (SAM), both in transmission and in reflection modes, has been widely discussed in the literature[1] and has been used to study the acoustic properties of various materials. It has been particularly interesting for surface and subsurface flaw detection[2] which is important in nondestructive evaluation (NDE). The best resolution yet achieved with such an instrument is comparable and even better than that of the optical microscope[3] and improvement is still to come. Imaging with the SAM is achieved by a raster scanning of the acoustic beam waist in the focal plane transverse to the beam axis; this can be performed in amplitude, phase or both at the same time.

In addition to the scanning mode, the SAM may be used to measure more directly the elastic properties; this is the acoustic material signature technique (AMS) which involves the translation of the sample, without scanning, along the axis from the focal plane toward the acoustic lens. It is possible from the amplitude of the AMS signal to measure the Rayleigh velocity[4] and the attenuation.[5–7] There is however more information to get if we plot at the same time the amplitude and phase of the AMS signal. In addition, if the scanning mode and the AMS technique are used simultaneously, it is possible to obtain acoustic images of curved surfaces[8] which represent a two-dimensional mapping of the AMS. In this paper we want to show how the full AMS, amplitude and phase, may be used to characterize nonplanar surfaces. In Sec. II we will briefly discuss the AMS signal and outline the elastic properties which can be measured from it. We describe in Sec. III the experimental setup used to obtain the full AMS and to image nonplanar surfaces. Some AMS signals and acoustic images are presented in Sec. IV for different planar and nonplanar surfaces; two interesting applications of the technique are described with acoustic images, characterization of small acoustic lenses and subsurface defects.

II. ACOUSTIC MATERIAL SIGNATURE (AMS)

In the pulsed reflection mode SAM, longitudinal waves emitted by a piezoelectric transducer are focalized by a wide angle lens on an object surface through a liquid (water); the waves reflected from this surface propagate back to the transducer and produce an output voltage. The AMS is the variation of this output voltage with distance z from the lens to the object surface for distances smaller than the focal length. A series of deep minima in the signal amplitude are noticed with a periodic spacing which depends on the Rayleigh velocity V_R when it is greater than the velocity in water V_w; for materials with $V_R < V_w$ it depends on the longitudinal wave velocity.[4]

The AMS signal has been tentatively explained to be the result of interference between the two components radiating in the liquid at the critical Rayleigh angle θ_R[4]: one component is specularly reflected from the solid and the second component undergoes a lateral shift before reradiating at θ_R, the shift being proportional to the axial translation Δz of the solid surface from the focal plane towards the lens. This model has been corrected by Parmon *et al.*[9] who have introduced a ray model which interprets the AMS as due to the interference between a narrow bundle of axial rays and rays associated with the leaky Rayleigh wave excited on the surface. The spacing between the minima is then shown to be given by

$$\Delta z = \frac{\lambda_R}{\sin\theta_R}\,\frac{1+\cos\theta_R}{2},$$

where λ_R is the Rayleigh wavelength. From a measurement of the spacing one obtains the mean Rayleigh velocity in the analyzed surface plane. This feature of the AMS is also used to measure the surface wave absorption, film thickness through dispersion of Rayleigh waves, texture of materials, etc. The AMS is responsible for the contrast in the acoustic images and this is why it is so important in the SAM. More information may be gathered on elastic properties by looking at the full AMS signal, i.e., amplitude and phase.

As it has been shown by Wickramasinghe[10] and Atalar[11] and angular spectrum approach may be used to derive an expression for the transducer output signal in terms of the reflectance function whose angular dependence is determined by the bulk constants of the material itself. This is how the contrast obtained in the reflection acoustic microscopy is explained. The transducer voltage is then expressed by the following relation[10]

[a] Institut de Génie des Matériaux, CNRC, Montréal, H4C 2K3 Québec, Canada.

 0021-8979/84/010089-05$02.40

$$V(z) = \int_0^\infty [P(\lambda\rho R)]^2 [u_1^+(\lambda\rho R)]^2 \times R(\rho) \exp[2k^1 z(1-\rho^2\lambda^2)^{1/2}] 2\pi\rho \, d\rho,$$

where k^1, λ, R, ρ, u_1^+, and P are, respectively, the propagation constant in the liquid, the wavelength in the liquid, the lens radius of curvature, the spatial frequency, the incoming acoustic field on the cavity, and the effective lens pupil function. The reflectivity function R is generally a strong function of the elastic constants and orientation of the material being imaged; information on this function must then be available from $V(z)$. This is what one does when the Rayleigh wave velocity and attenuation are measured from the usual AMS (amplitude). But more information may be gathered with the full AMS signal, amplitude and phase, given by the real and imaginary parts of $V(z)$. These parts of $V(z)$ are measured by mixing at the same frequency a cw reference signal with the output signal of the transducer. The experimental procedure is described in the next section and the results will be shortly discussed (Sec. IV).

III. EXPERIMENTAL SETUP

The SAM used for this study has been described elsewhere[12] and it is working in the pulsed reflection mode at 150 and 450 MHz. The AMS signals are obtained with the schematic setup shown in Fig. 1. The transducer output signal goes in the detection arm of the SAM: it passes through rf amplifiers before entering a wideband mixer. A cw reference signal at the same frequency is then mixed with the acoustic signal. The mixer's output goes in a boxcar integrator in order to select the focalization pulse. The $V(z)$ curve is obtained on an X–Y recorder: the integrator output is directed on the Y axis and a position signal coming from a linear voltage differential transducer (LVDT) mounted along the axis of the sample holder is put on the X axis. If the setup is used for imaging, the integrator output is registered for each pulse in a digital memory in synchronization with the raster scan pattern.

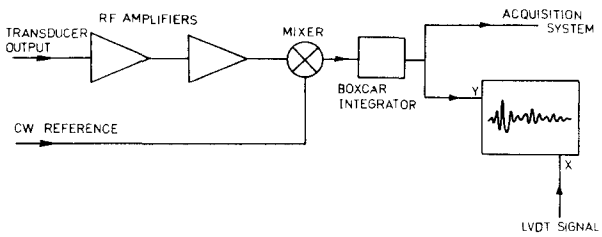

FIG. 1. Experimental setup for AMS recording and imaging.

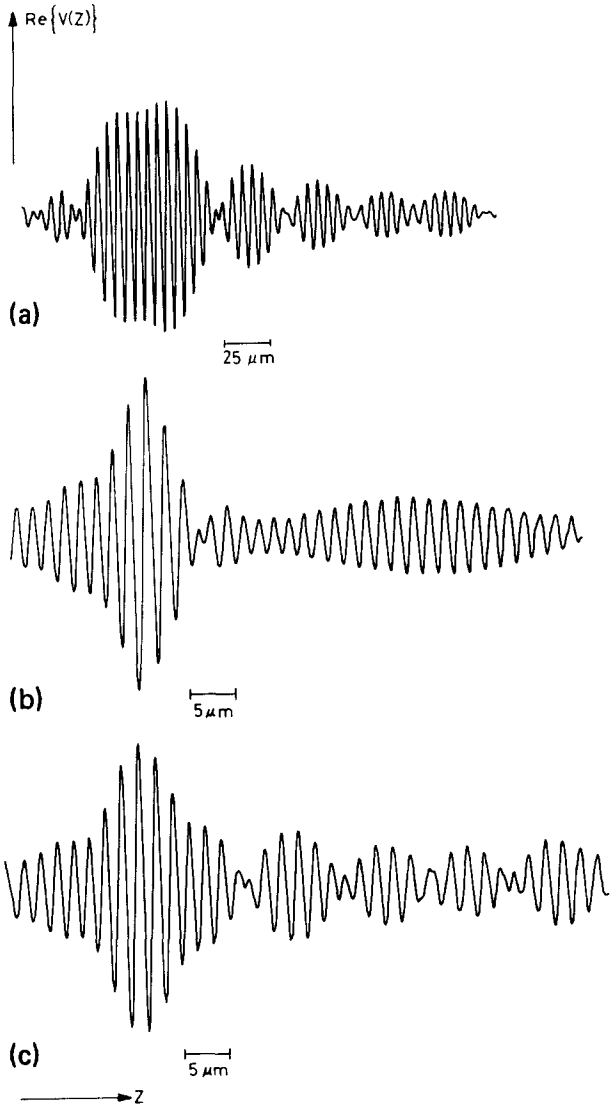

FIG. 2. Acoustic material signatures (AMS). (a) Duralumin planar surface at 150 MHz, (b) Al_2O_3 (c) planar surface-gold film (1500 Å) at 450 MHz, (c) Al_2O_3 (c) planar surface-gold film (1500 Å)-ZnO film (3.5 μm) at 450 MHz.

IV. RESULTS

A. AMS Signals on planar surfaces

We present in Fig. 2 the AMS signals obtained on different planar surfaces with the experimental setup of Fig. 1. The AMS were obtained at 150 MHz for the isotropic duralumin surface (a) and at 450 MHz for the Al_2O_3-gold surface (b) and the Al_2O_3-gold-ZnO interface (c). In the last AMS, the ZnO piezoelectric film is 3.5-μm thick and it was rf sputtered on Al_2O_3 in order to make a compression wave transducer; the film is polycrystalline and preferentially oriented to generate compressionnal waves.

The AMS signals at both frequencies show the same overall feature, a fast varying signal which is amplitude modulated with decreasing intensity as the distance separating the sample from the lens is shortened. The amplitude modulation gives the interference minima which are observed in the usual AMS and it may serve to measure the Rayleigh velocity and critical angle. The fast varying signal has an "effective wavelength" which is slightly changing over the complete AMS and it is approximatively given by $\lambda/2$ (λ is the acoustic wavelength in water) corrected by a cosine factor; when the spacing z is changed by $\sim\lambda/2$, the path difference for the reflected signal is $\sim\lambda$ and the phase has changed by 2π. This situation is valid for small angles and if we want to take care of all the angular spectrum, a cosine factor will be introduced. Three angles are important to determine this

factor, the small angles (0°), the Rayleigh critical angle and the maximum aperture angle θ_M, with different weight as defocalization proceeds. In Fig. 2(a), the effective wavelength is 5.44 μm ($\lambda/2$ is 5.00 μm at 150 MHz) and the effective angle is 30°; for Al_2O_3-gold [Fig. 2(b)] and Al_2O_3-gold-ZnO [Fig. 2(c)], we find 1.73 μm ($\overline{\theta} \simeq 15.1°$) and 1.85 μm ($\overline{\theta} \simeq 25.5°$) with $\lambda/2 = 1.67\,\mu$m at 450 MHz. For these three planar surfaces the mean Rayleigh angles are, respectively, 30°, 15.3°, and 32.5°; the aperture angle being $\simeq 51.5°$ for both lenses, it seems that the most important contribution to the effective wavelength comes from the small and Rayleigh angles. From such a study one can appreciate the role played by the reflectivity function in the expression for $V(z)$. By measuring with precision this effective wavelength as the lens-to-sample spacing is shortened, we obtained a calibration AMS which will serve to interpret subsequently the acoustic images on nonplanar surfaces.

B. Applications to nonplanar surface characterization

We will now show some applicaltions of the AMS signal, amplitude and phase, for imaging nonplanar surfaces. Weglein[8] has done the acoustic microscopy of curved surfaces by using simultaneously the two operation modes of the SAM when a nonplanar sample of known curvature is raster scanned. It has been suggested that the obtained images represent a two-dimensional mapping of the AMS, specifying the Rayleigh wave velocity and its spatial variation in the image area. An acoustic image of a ball bearing,[8] for example, showed a set of nearly concentric bright and dark rings whose number depends on the distance of the spherical surface from the lens and may attain a maximum equal to the number of periods in the one-dimensional AMS done in amplitude. We want to show here how the full AMS may be used in the same way to study nonplanar surface with more sensitivity. We show in Fig. 3 the acoustic image (150 MHz) of a concave spherical cavity ($R_0 \simeq 215\,\mu$m) ground and polished in an Al_2O_3 buffer (**c** axis oriented) which will be used for an acoustic lens at 450 MHz. A smaller cavity ($R_0 \simeq 80\,\mu$m) has also been imaged acoustically at 150 MHz on a similar buffer and it is shown in Fig. 4. For both cavities a series of concentric bright and dark rings appear on the acoustic image over the cavity aperture and these are the result of the fast varying signal appearing in the AMS. The ring formation is explained in Fig. 5. We register first the one-dimensional AMS signal [Fig. 5(a)] obtained on the spherical cavity in order to get a spatial calibration; this is important since the Rayleigh velocity on a concave spherical surface is different from a planar one. Then, having chosen the adequate focalization on the cavity, the acoustic beam is raster scanned in order to obtain the full image [Fig. 5(b)]. Because the surface is nonplanar, the fast varying signal will produce a set of concentric rings on the image [Fig. 5(c)]. The intensity of the rings is decreasing rapidly because of divergence of the acoustic beam on such a spherical surface and the intensity is modulated according to the usual signature modulation. These observations may all be checked on the acoustic images shown in Figs. 3 and 4.

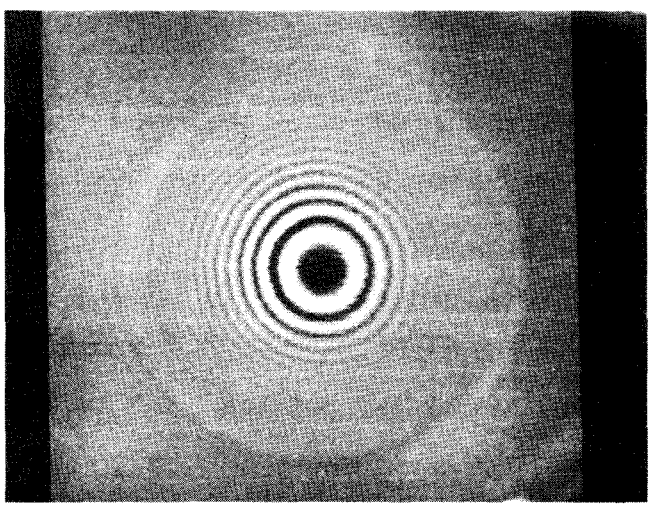

FIG. 3. Acoustic image of a spherical cavity ground and polished in an Al_2O_3 (**c**) buffer. $R_0 \simeq 215\,\mu$m, $f = 150$ MHz. Field of view $512 \times 515\,\mu$m^2.

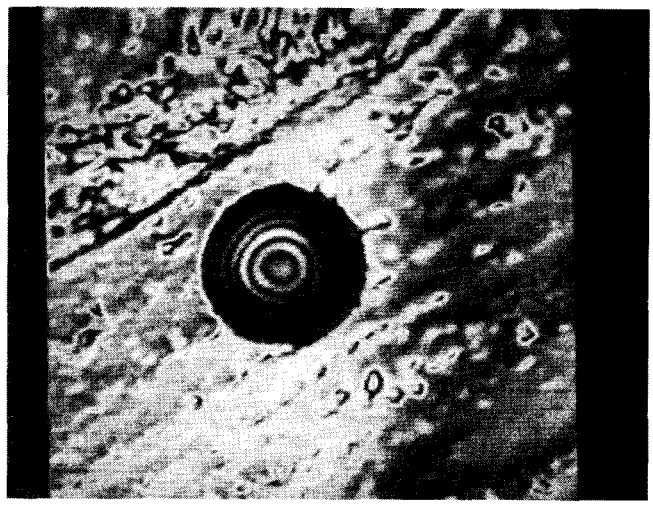

FIG. 4. Acoustic image of a spherical cavity ground and polished in an Al_2O_3 (**c**) buffer. $R_0 = 80\,\mu$m, $f = 150$ MHz. Field of view $512 \times 512\,\mu$m^2.

In order to have a good working lens in the SAM without aberration, the spherical cavity must be perfectly ground and polished. With the images shown here it is thus possible to verify the quality and sphericity of the lens by measuring the radii of the rings and by reconstructing the cavity with the calibration AMS. This has been done on several of our lens with high efficiency. Smaller lenses have to be imaged at higher frequency in order to obtain more rings and to improve resolution. When the cavity is reconstructed, we can determined the exact radius of curvature and the focal length; this last parameter may also be obtained from the folded reflection signal on the AMS appearing at z equal to half the focal length when the lens is itself used. All the important parameters of the lens may thus be checked with the acoustic images.

The same technique may also be used for subsurface defect characterization. Here the acoustic beam is focalized inside the solid sample on a particular defect to be imaged.

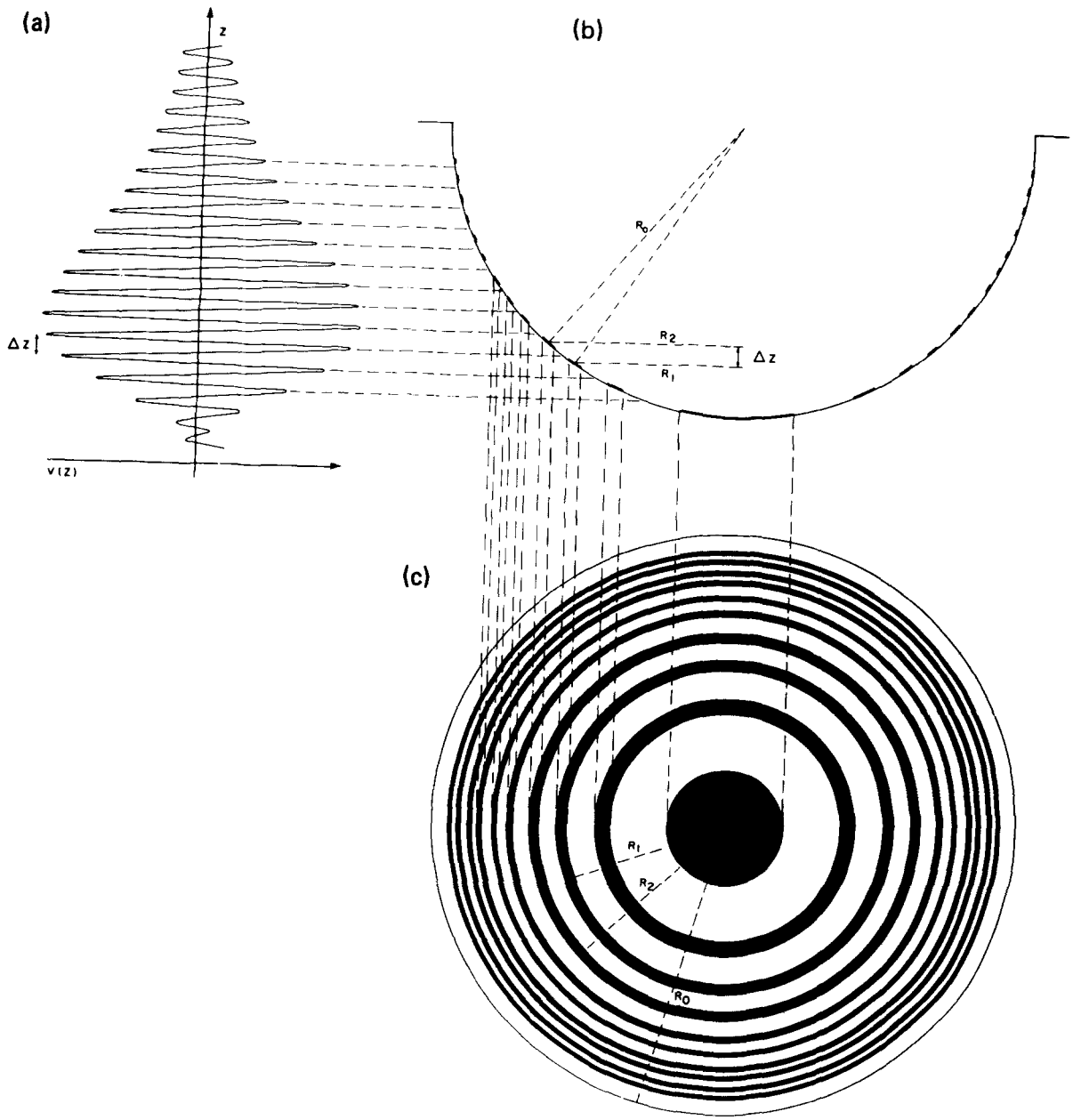

FIG. 5. AMS imaging of a concave spherical surface at 150 MHz. (a) One-dimensional AMS obtained on a concave spherical surface, (b) scanning of one line over the concave spherical surface, (c) complete acoustic image: when the lens-to-surface spacing is changed by Δz equal to the effective wavelength, a bright or dark ring appears. By measuring R_1, R_2, etc., the radii of the rings, one can reconstruct the profile of the nonplanar surface.

By gating the appropriate reflected pulse on the defect, we obtain the signal $V(z)$, amplitude, and phase, in the same way used for planar or nonplanar surfaces and described preceedingly. For subsurface defect the main difference lies in the fact that the interface over which the acoustic beam will be scanned, is quite different in nature; here the acoustic pulse reflects on a solid-defect interface rather than a water-solid one. Consequently the fast varying signal $V(z)$ will present an effective wavelength that will be determined by $\lambda_{\text{solid}}/2$ instead of $\lambda_{\text{water}}/2$, λ_{solid} being the acoustic wavelength in the solid, either longitudinal or transverse. According to this picture the acoustic image of a subsurface defect should present a fringe pattern which will be similar to what is found for a nonplanar surface, but the fringe spacing will be related to the acoustic wavelength in the solid rather than water. We have reported previously[12] acoustic images of subsurface defects which were presenting fringe patterns although these images were done in amplitude only. We since found out that a small cw leakage signal was detected at the transducer at that time so as to give both the phase and amplitude of $V(z)$. These images have since been redone with the setup of Fig. 1 and they show now very contrasted fringe patterns around the various defects. We present in Fig. 6 the acoustic image of a cylindrical (and conical) hole drilled in a duralumin buff-

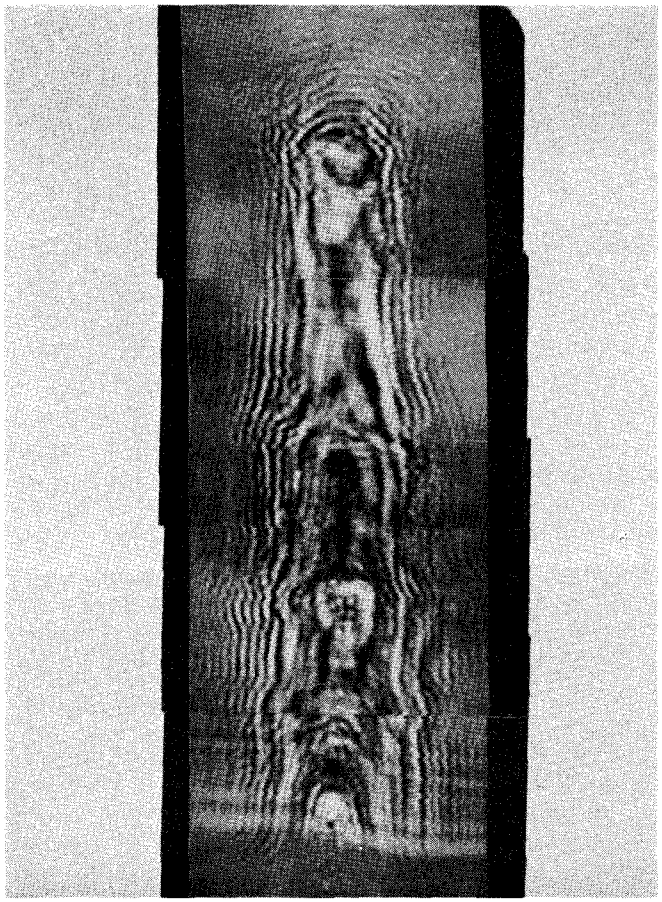

FIG. 6. AMS imaging of a subsurface defect at 150 MHz: drilled hole under the surface of a duralumin planar surface. Diameter$\simeq$475 μm, depth$\simeq$90 μm. Field of view 0.5×1.5 mm^2.

er surface and filled with air (diameter$\simeq$280 μm, depth$\simeq$90 μm); the image was obtained at 150 MHz with the transverse acoustic pulse. The alternating bright and dark fringes are the result of the fast varying signal $V(z)$; the fringe spacing is consistent with the wavelength of the transverse reflected acoustic pulse. We should notice that the fringe pattern gives the exact shape of profile of the hole, especially the successive steps of drilling because of technical difficulties which explain why the outside diameter is larger ($\sim$475 μm) than expected. To reconstruct the profile of the defect one has to obtain first the calibration AMS at the duralumin-air interface which constitutes the defect and subsequently use the fringe pattern to characterize the defect. Similar fringe patterns have also been observed with the SAM around surface cracks.[13] They were however produced by an interference phenomenon between the leaky Rayleigh waves reflected on the crack and the normal reflected acoustic waves at the interface. Even if these patterns and the one described in this paper are quite different in nature, they are both very useful to characterize surface and subsurface defects with a high resolution and contrast.

V. CONCLUSION

We have shown in this paper how the two operation modes of a pulsed reflection type SAM, one-dimensional AMS and raster scanning, are used simultaneously to characterize nonplanar surfaces. In the nonscanning mode the full AMS signal (amplitude and phase) is used to determine the Rayleigh velocity and to measure the influence of the reflectivity function of planar surfaces. In the raster scanning mode, the acoustic image shows fringe patterns on nonplanar surfaces which can be used, together with a calibration one-dimensional AMS, to characterize the profile and shape of the surface or subsurface defect. These fringe patterns constitute also a two-dimensional map of the elastic parameters distribution of the surface to be imaged. This technique has been applied with success to check the sphericity of small acoustic lenses; it has been also applied to subsurface defect detection and characterization in a duralumin buffer.

ACKNOWLEDGMENTS

This work has been supported by the National Research Council of Canada through its Institut de Génie des Matériaux. The authors thank Professor H. K. Wickramasinghe for suggesting the measurement of the full AMS.

[1]C. Quate, A. Atalar, and H. K. Wickramasinghe, Proc. IEEE **67**, 1092 (1979).
[2]C. S. Tsai, S. K. Wang, and C. C. Lee, Appl. Phys. Lett. **31**, 317 (1977).
[3]J. Heiserman, in *Scanned Image Microscopy* (Academic, New York, 1980).
[4]R. D. Weglein, Appl. Phys. Lett. **34**, 179 (1979).
[5]R. D. Weglein, Electron. Lett. **18**, 20 (1981).
[6]K. Yamanaka, Electron. Lett. **18**, 587 (1982).
[7]I. R. Smith and H. K. Wickramasinghe, Electron. Lett. **18**, 955 (1982).
[8]R. D. Weglein, Appl. Phys. Lett. **38**, 516 (1981).
[9]W. Parmon and H. L. Bertoni, Electron. Lett. **14**, 305 (1978).
[10]H. K. Wickramasinghe, Electron. Lett. **14**, 5130 (1978).
[11]A. Atalar, J. Appl. Phys. **49**, 5130 (1978).
[12]M. Poirier and J. D. N. Cheeke, *Proceedings of the 1982 IEEE Ultrasonics Symposium* (IEEE, New York, 1982), p. 640.
[13]K. Yamanaka and Y. Enomoto, J. Appl. Phys. **53**, 845 (1982).